Lattice orientation effect on the nanovoid growth in copper under shock loading

Wenjun Zhu,[1,2,*] Zhengfei Song,[1] Xiaoliang Deng,[1,2] Hongliang He,[1] and Xiaoyin Cheng[3]
[1]*Laboratory for Shock Wave and Detonation Physics Research, Institute of Fluid Physics, Mianyang 621900, People's Republic of China*
[2]*Department of Physics, Sichuan University, Chengdu 610065, People's Republic of China*
[3]*Nanotechnology Center, ITC, The Hong Kong Polytechnic University, Kowloon, Hong Kong*
(Received 10 March 2006; revised manuscript received 9 August 2006; published 8 January 2007)

Molecular-dynamics (MD) simulations have revealed that under shock loading a nanovoid in copper grows to be of ellipsoidal shape and different loading directions ([100] and $[1\bar{1}1]$) change the orientation of its major axis. This anisotropic growth is caused by preferential shear dislocation loop emission from the equator of the void under [100] loading and preferential shear dislocation loop emission deviating away from the equator under $[1\bar{1}1]$ loading. A two-dimensional stress model has been proposed to explain the anisotropic plasticity. It is found that the loading direction changes the distribution of the resolved shear stress along the slip plane around the void and induces different dislocation emission mechanisms.

DOI: 10.1103/PhysRevB.75.024104 PACS number(s): 61.72.Qq, 62.20.Mk, 62.50.+p, 62.20.Fe

Void nucleation, growth, and coalescence have long been realized to play a critical role in the initiation of dynamic failure in ductile metals.[1,2] The nucleation can initiate from preexisting defects, such as grain boundaries, vacancies, voids, inclusions, etc. under shock loading.[3] Once voids have been formed, they will grow in size and interact with each other, leading to a dynamic fracture. Single void growth models based on continuum theory are extensively employed to investigate shock induced spallation phenomena.[4–9] Although this continuum damage model (CDM) can reproduce the free-surface velocity of experiments well, it ignores the discrete nature of metals and the mechanism of plasticity. It is also questionable to apply this model to microscopic length and time scales that belong to the incipient stage of void growth. In the absence of experimental information, in recent years, atomistic simulations of nanovoid growth have been carried out to investigate the incipient stage of the void growth and the corresponding mechanisms,[10–13] even the coalescence process.[14] But their loading conditions have been either quasistatic or strain-rate controlled, which does not take into account the inertial effect.[15,16] Furthermore, the lattice orientation with respect to loading direction has not yet been considered. Recent laser shock experiments illustrated that at high strain rate conditions vacancy diffusion mechanism cannot explain the void fraction in recovered samples, and both prismatic and shear dislocation loop emission mechanisms have been proposed to accommodate the void growth under shock loading.[17] But there is still no direct observation of the dynamic process of void growth under shock loading. In polycrystalline metals, each grain has a unique loading direction. How the shock loading direction affects the void growth remains unresolved so far. The main purpose of this work is to study the mechanism of the incipient stage of nanovoid growth under shock loading and how the lattice orientation influences single void growth in monocrystal copper by means of molecular dynamics (MD) simulation.

The interaction between atoms is described by an embedded atom model (EAM) potential parametrized by Mishin,[18] and the potential not only reproduces mechanical properties including elastic constant, cohesive energy, defect formation energy, etc. at ambient condition, but also predicts the equation of state (EOS) of copper quite well under pressures up to 250 GPa. Shock loading directions have been chosen to be the [100] and $[1\bar{1}1]$ crystallographic directions. The x,y,z axes of the simulation boxes coincide with the [100], [010], [001] and $[1\bar{1}1]$, [110], $[\bar{1}12]$ for [100] and $[1\bar{1}1]$ crystalline directions, respectively. Periodical boundary conditions are applied to the y and z directions to mimic the uniaxial strain condition of planar shock loading. A nanovoid with a diameter of 1.5 nm is dug out at the center of the crystal. Shock waves are generated by taking two surface layers at one end of the sample as a piston and pushing the piston inward at a certain velocity. The piston velocity refers to the particle velocity behind the shock wave. The average stress along the loading direction stays constant behind the shock front and is usually referred to as the shock strength. Once the shock wave reaches the opposite free surface, the piston atoms are released. The rarefaction waves originate from both free surfaces and move into the crystal in opposite directions. Because the particle velocities behind the two rarefaction waves are different (in the center of mass frame, the velocities are equal in magnitude but opposite in sign), when they meet inside the crystal a tensile state is generated. We do not consider the temperature effect in this work, and the initial temperature is set as 0 K. Since the elastic precursor of shock wave along the $[1\bar{1}1]$ loading direction is faster than that along the [100] loading direction,[19] in order to exert the same tensile duration for the void, the dimensions of the single crystal for the [100] loading are set up as 17.2 nm$\times$16.3 nm$\times$16.3 nm or $47.5[100]\times45[010]\times45[001]$ containing 384 663 atoms and those for the $[1\bar{1}1]$ direction are taken as 20.0 nm$\times$17.9 nm$\times$15.5 nm or $32[1\bar{1}1]\times35[110]\times17.5[\bar{1}12]$ containing 470 308 atoms. The trajectory of each atom is integrated by a predict-correct scheme at a time step of 1 fs. Dislocation cores and stacking faults are identified by the pair analysis technique.[20]

Previous researches[21,22] have revealed void collapses induced by shock compression through dislocation emission

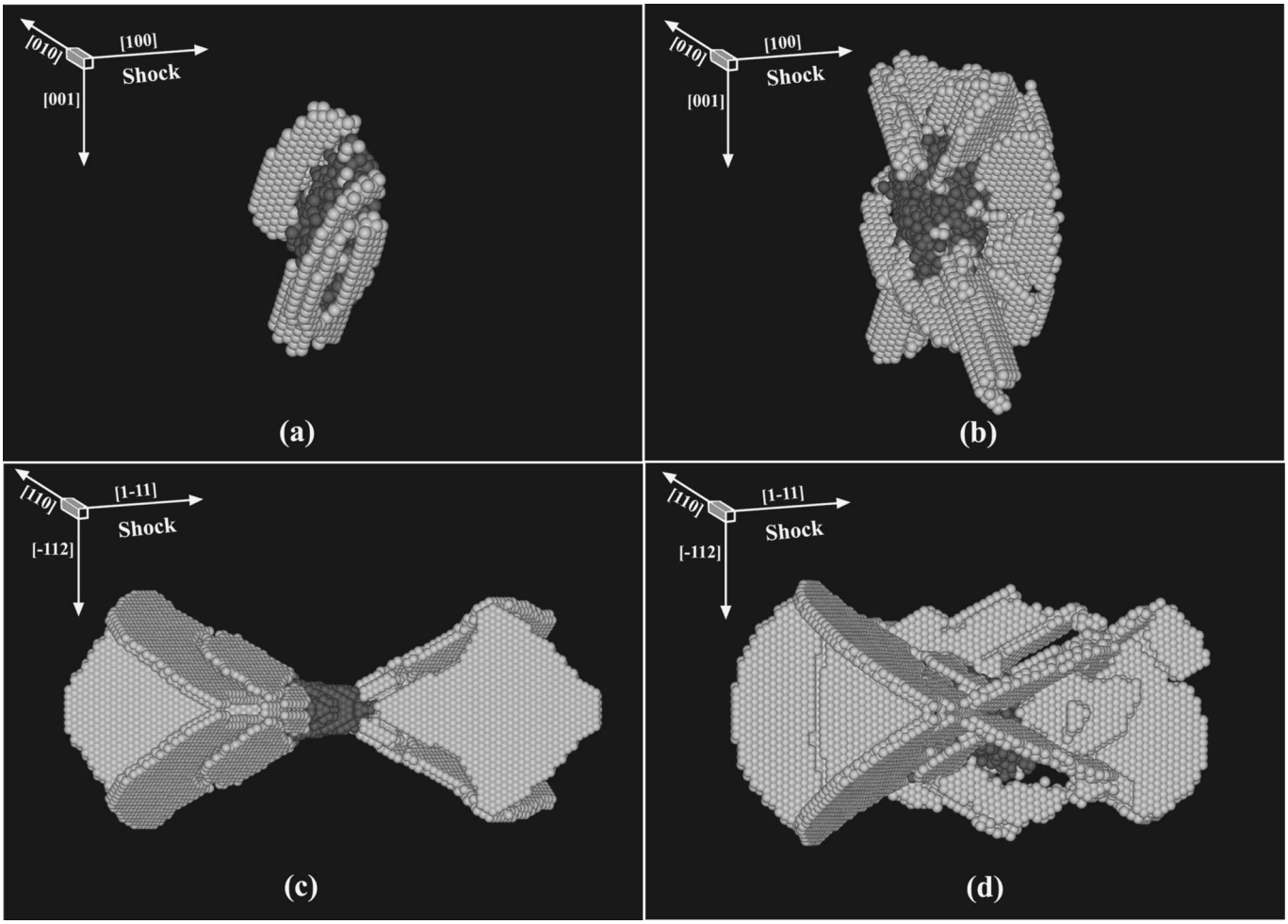

FIG. 1. Snapshots from MD simulations, showing associated plasticity of void growth under different loading direction and shock strength. The initial void diameter is 1.5 nm. Only atoms with hexagonal close-packed (HCP) structure (light gray) and amorphous structure (dark gray) are shown. The times for the snapshots are 8 ps after the simulations start. (a) 17.5 GPa shock strength and the [100] loading direction. (b) 20 GPa shock strength and the [100] loading direction. For (a) and (b), shear dislocation loops preferentially emit from equator region. (c) 20 GPa shock strength and the $[1\bar{1}1]$ loading direction. (d) 23.5 GPa shock strength and the $[1\bar{1}1]$ loading direction. For (c) and (d), the tetrahedron configurations formed by shear dislocation loops are predominantly emitted.

and shown that there exists a critical shock strength for the collapse of voids with a certain radius. By increasing the shock strength to exceed 17 GPa for each loading direction, we also observed that dislocations; are activated as the void collapses by shock compression. Since the $1/6\langle 211\rangle$ $\{111\}$ partial dislocation is the energetically favorite dislocation in face-centered cubic (FCC) structure, once the partial dislocation moves forward on a $\{111\}$ plane it leaves behind a stacking fault.[23] For the [100] loading direction, after the shock front sweeps over the void, shear dislocation loops are emitted from void surface on four different but equivalent $\{111\}$ slip planes. The shear dislocation loop expands outward and interacts with others to form stair-rod dislocations, these sessile dislocations limit the shape of the dislocation loop. On the leading side (which shock first hits) and the trailing side, the shear dislocation loops easily form four sides of a pentahedron with fourfold symmetry with respect to the loading direction. This characteristic phenomenon was also observed by Davila[21] and Hatano's[22] simulation. For the $[1\bar{1}1]$ direction, because the resolved shear stress is zero on the $(1\bar{1}1)$ plane, the shear dislocation loops on other three $\{111\}$-type planes can interact and easily form three sides of a tetrahedron with threefold symmetry to the loading direction. After the rarefaction waves interact inside crystal and the tensile state is generated around the void, the leading partials of shear dislocation loops reverse their movement causing annihilation of the stacking faults and unzipping of the stair-rod dislocation as the void expands. Almost all the trace of plasticity during compression, including stacking fault and dislocation, disappear when the void bounces back to its original size and shape (see Fig. 2). The recovery process does not leave any residual dislocations. This is not like Marian's[11] quasistatic simulation of a nanovoid deformation subjected to cyclic shear loading in Al. We believe one reason for this is that copper has a low stacking fault energy and between the trailing and the leading dislocations there is a large stacking fault area; the compression period is not long enough for us to observe the trailing dislocation coming out from the surface. Another reason is that the shock strength is not strong enough to produce cross slips and jogs, because if

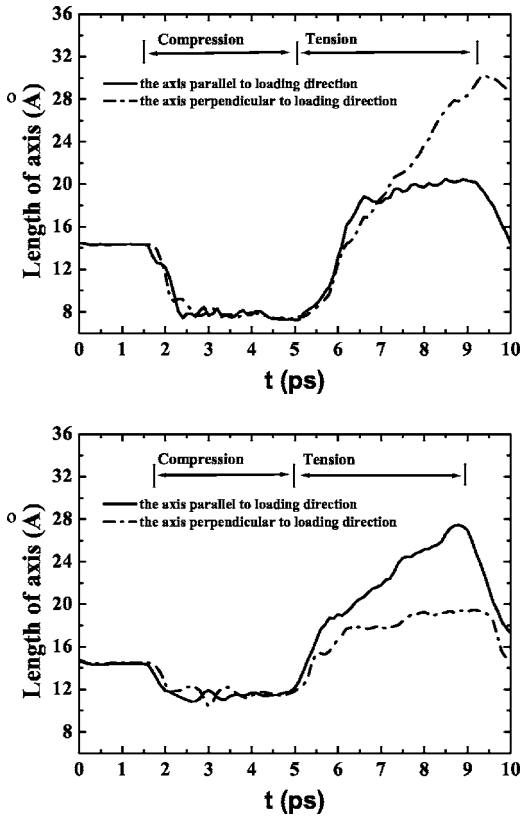

FIG. 2. The evolution of the axes of the void. The solid line represents the evolution of the axis paralleling to the loading direction and the dash-dotted line is for the axis perpendicular to the loading direction. The initial length of both axes is 15 Å. (a) 17.5 GPa shock strength and the [100] loading direction. (b) 20 GPa shock strength and the $[1\bar{1}1]$ loading direction.

the shock strength exceeds 25 GPa the corresponding tensile stress will induce more voids, which is beyond the scope of this paper. Since our attention is focused on a single void growth, without considering any residual dislocations left from the compression process we can simplify the analysis for the following phenomenon. As the void further expands to exceed its elastic limit, it will emit dislocations. During this plastic growth, our simulations for the [100] and $[1\bar{1}1]$ loading directions show different dislocation emission pattern and the spherical void changes into different shapes.

Figure 1 shows snapshots of the plasticity associated with the void growth under both [100] and $[1\bar{1}1]$ loading conditions. For the [100] loading condition, first we observe the dislocation nucleate from the equator of the void perpendicular to the loading direction. As the void grows, the nucleated dislocations expand outward to form shear dislocation loops. Driven by stronger shock strength, the void grows faster and more shear dislocation loops emit from the surface. Some of the loops meet and interact with each other to form sessile stair rod dislocations, blocking further movement, and a pentahedron configuration with fourfold symmetry with respect to the loading direction is also observed. However the shear dislocation loops emitting from the equator are dominant and move faster than those in other regions. This mechanism makes the void grow preferentially along the direction perpendicular to the loading direction. The shape of the void can be represented by the axes of the void. Figure 2 shows the time history of the axes of the void. During the elastic expansion, the void becomes ellipsoidal and its major axis is parallel to the loading direction. After the void grows

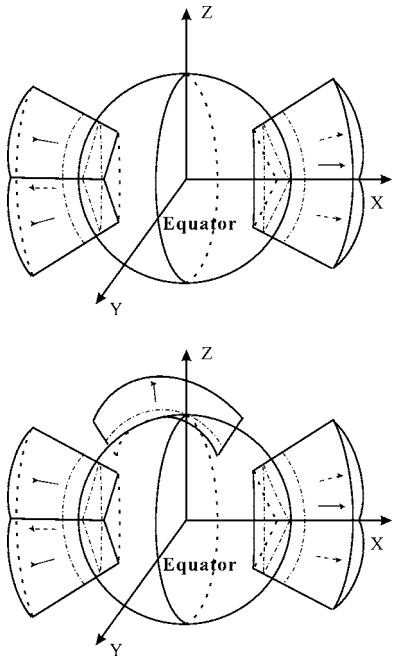

FIG. 3. A three-dimensional illustration of the mechanisms of the void growth for the $[1\bar{1}1]$ loading direction. (a) When the shock strength is below 22 GPa, the sectors of surface enclosed by each three shear dislocation loops forming three sides of a tetrahedron configuration are pulled out as the loops expand outward. (b) When the shock strength exceeds 22 GPa, besides the tetrahedron configuration there are more shear dislocation loops emitting from the equator region (only one shear dislocation loop cross the equator is illustrated).

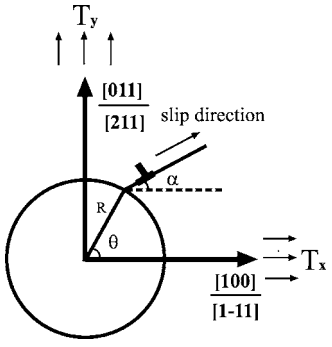

FIG. 4. A two dimensional representation of a stress-free hole in infinite medium under uniform biaxial far-field tension. T_x and T_y are biaxial far field tension. Under uniaxial strain condition, $T_x > T_y$. Only one of the slip family planes is shown. When the [100] and [011] coincide with x and y axes, respectively, the condition corresponds to the [100] loading condition. When $[1\bar{1}1]$ and [211] coincide with x and y axes, respectively, the condition corresponds to the $[1\bar{1}1]$ loading condition. The slip plane has an angle of α with loading direction. R is the radius of the cylinder void.

plastically, the major axis changes the orientation to being perpendicular to the loading direction.

As for the $[1\bar{1}1]$ loading direction, the resolved shear stress on $(1\bar{1}1)$ plane is zero and there is no slip being activated on this family of planes. It is very interesting to observe two stages of void growth. When the shock strength is below 22 GPa, the dislocations nucleate from edges of two triangle sites away from the equator (each triangle is located on opposite surfaces of the void along the loading direction). Then the three dislocations initiating from each triangle move outward on {111} planes, interacting with each other and forming sessile stair-rod dislocation. In this way these dislocation loops form two tetrahedron configurations with threefold symmetry to the loading direction gliding away from the void on opposite directions along $[1\bar{1}1]$ [see Fig. 1(c)]. As the dislocation loops move away, the sector of the void's surface surrounded by the dislocation loops is punched out along the loading direction. If the shock strength is increased to more than 22 GPa, besides the tetrahedrons formed by shear dislocation loops, shear dislocation loops are also observed to originate from the equator of the void. Because the dislocation loops on sides of the tetrahedrons move faster than the dislocation loops generated from the equator, the major axis of the ellipsoidal void remains paralleling to the loading direction. Figure 3 illustrates this two stage void growth mechanisms. In order to check the size effect, we increase the length of the y and z dimensions by 50%. For the [100] direction, the dimensions of crystal are set as $47.5[100]\times55[010]\times55[001]$ containing 574 663 atoms and for the $[1\bar{1}1]$ direction are set as $32[1\bar{1}1]\times42[110]\times21.5[\bar{1}12]$ containing 693 508 atoms, and the dislocation emission pattern and shape evolution of the void are similar to those of the smaller size simulation.

Why is the plastic mechanism of the void growth different for the [100] and $[1\bar{1}1]$ loading directions? Since the dislocation generation and movement depend on shear stress, the distribution of the resolved shear stress along the slip planes around the void surface is critical to understand the above plastic phenomena. At the atomistic scale, the local stress should be obtained by spatially averaging the virial stress[24] over a characteristic volume,[25,26] which is usually more than a 4 unit cell. Therefore, the stress distribution calculated by the above method is rough for the nanovoid. Alternatively, we observed that when the void expands to its elastic limit, the tensile wave fronts already have a distance of more than 5 times the void radius away from the void surface. In spite of the inertial effect near the void surface, we propose the void is subjected to a static biaxial far-field tension. Because the two-dimensional problem can be solved analytically, we simplify the three-dimensional problem to a two-dimensional problem as a stress-free hole in an infinite medium under biaxial tension as illustrated in Fig. 4. The analytical stress distribution on the surface of the stress-free hole under uniform tension along one direction can be represented as $\sigma_R=\tau_{R\theta}=0$ and $\sigma_\theta=T_x(1-2\cos 2\theta)$, where T_x is the far-field tension.[27] Considering uniaxial strain condition of shock loading, the tensile strength perpendicular to the loading direction satisfies $T_y=kT_x$, where k is a biaxial loading ratio, then on the surface of the void $\sigma_\theta=T_x[2(k-1)\cos 2\theta+(1+k)]$. The stress σ_θ is maximum at $\theta=\pm\pi/2$ regardless of what the loading direction is, corresponding to the equator of the void. However, only the resolved shear stress along the slip direction contributes to the nucleation and emission of dislocations. If we define α as the angle between the slip plane and the loading direction, the distribution of resolved shear stress along this slip direction around the cylinder surface is

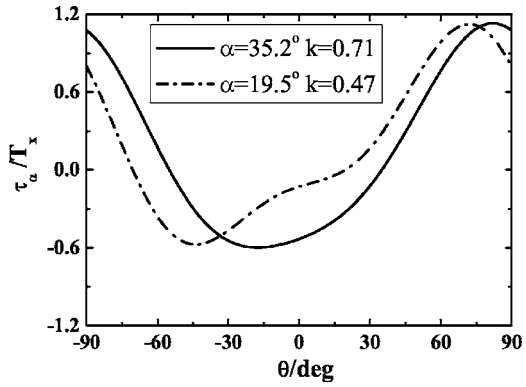

FIG. 5. The distribution of the resolved shear stress along the slip plane on the surface of cylinder void in infinite medium under biaxial far field tension. T_x and T_y are the far field tensions along and perpendicular to the loading direction, respectively. The biaxial loading ratio is $k=T_y/T_x$. The solid line represents the condition that the slip plane has an angle of 35.2° with respect to the loading direction and k is 0.71. The dash-dotted line represents the condition that the slip plane has an angle of 19.5° with respect to the loading direction and k is 0.47.

$$\tau_\alpha=\frac{1}{2}T_x[2(k-1)\cos 2\theta+(1+k)]\sin 2(\alpha-\theta). \quad (1)$$

Figure 5 shows the variation of τ_α with θ. For the [100] loading direction, the angle between {111} family planes [except $(1\bar{1}1)$ plane] and the loading direction is $\alpha=35.2°$. According to the elastic constants of single crystal copper on ambient condition, $c_{11}=168.0$ GPa, $c_{12}=122.6$ GPa, $c_{44}=75.3$ GPa,[28] the biaxial loading ratio for uniaxial strain condition is estimated to be $k=\frac{c_{12}}{c_{11}}\approx0.71$. So the maximum value of τ_α is at $\theta\approx85°$, which corresponds to the location of the void surface very close to the equator. As for the $[1\bar{1}1]$ loading direction, α is 19.5° and $k=(c_{11}+2c_{12}-2c_{44}/c_{11}+2c_{12}+2c_{44})\approx0.47$, the maximum value of τ_α is at $\theta\approx74°$, which is further away from the equator compared with the [100] loading condition. That is why we observe the dislocations nucleate favorably at the equator for [100] loading. Furthermore, both α and θ are smaller for $[1\bar{1}1]$ loading conditions, the emitted dislocations are closer to each other and easier to form tetrahedron configuration. By increasing tensile strength, dislocations can emit from everywhere from the void surface. But the concentration of resolved shear stress τ_α favor the shear dislocation loop emission from the equator for the [100] loading condition and shear dislocation loop emission away from the equator for the $[1\bar{1}1]$ loading

condition, which leads to preferential growth toward the direction perpendicular and parallel to the loading direction, respectively.

In summary, we have performed MD simulations to reveal the anisotropic incipient plastic phenomenon of single nanovoid growth in single copper crystal under different shock loading direction. A two-dimensional resolved shear stress model has been derived to reveal that the angle between slip planes and loading direction and anisotropic elastic response of single crystal copper change the concentration of resolved shear stress around the void, which contributes to the anisotropic nanovoid growth and its associated plasticity. Although these simulation and analyses are carried out for an FCC metal (Cu), it has implications for other crystalline materials. The lattice orientation effects have been found to influence the single void growth, and is believed to have an affect on void coalescence as well.

The research was supported by NASF Project No. 10476027 of the National Natural Science Foundation of China and by Grant No. 20050105 from the Science and Technology Foundation of China Academy of Engineering Physics. The authors would like to thank Min Zhou and Fuqian Jing for helpful discussions.

*Electronic mail: wjzhu@caep.ac.cn

[1] M. A. Meyers, *Dynamic Behavior of Materials* (John Wiley & Sons, Inc., New York, 1984), Chap. 16.8, p. 523.
[2] L. Seaman, D. R. Curran, and D. A. Shockey, J. Appl. Phys. **47**, 4814 (1976).
[3] D. R. Curran, L. Seaman, and D. A. Shockey, Phys. Rep. **147**, 253 (1987).
[4] T. W. Barbee, L. Seaman, R. Crewdson, and D. Curran, J. Mater. **7**, 393 (1972).
[5] M. M. Carroll and A. C. Holt, J. Appl. Phys. **43**, 1626 (1972).
[6] J. N. Johnson and F. L. Addessio, J. Appl. Phys. **64**, 6699 (1988).
[7] J. R. Rice and D. M. Tracey, J. Mech. Phys. Solids **17**, 201 (1969).
[8] J. P. Feng, F. Q. Jing, and G. R. Zhang, J. Appl. Phys. **81**, 2575 (1997).
[9] G. Z. Voyiadijis, A. N. Palazotto, and X-L Gao, Appl. Mech. Rev. **55**, 481 (2002).
[10] J. Marian, J. Knap, and M. Ortiz, Phys. Rev. Lett. **93**, 165503 (2004).
[11] J. Marian, J. Knap, and M. Ortiz, Acta Mater. **53**, 2893 (2005).
[12] R. E. Rudd and J. Belak, Comput. Mater. Sci. **24**, 148 (2002).
[13] E. T. Seppala, J. Belak, and R. E. Rudd, Phys. Rev. B **69**, 134101 (2004).
[14] E. T. Seppala, J. Belak, and R. E. Rudd, Phys. Rev. Lett. **93**, 245503 (2004).
[15] M. Ortiz and A. Molinari, J. Appl. Mech. **59**, 48 (1992).
[16] P. F. Thomason, Acta Mater. **47**, 3633 (1999).
[17] V. A. Lubarda, M. S. Schneider, D. H. Kalantar, B. A. Remington, and M. A. Meyers, Acta Mater. **52**, 1397 (2004).
[18] Y. Mishin, M. J. Mehl, D. A. Papaconstantopoulos, A. F. Voter, and J. D. Kress, Phys. Rev. B **63**, 224106 (2001).
[19] E. M. Bringa, J. U. Cazamias, P. Erhart, J. Stolken, N. Tanushev, B. D. Wirth, R. E. Rudd, and M. J. Caturla, J. Appl. Phys. **96**, 3793 (2004).
[20] J. D. Honeycutt and H. C. Anderen, J. Phys. Chem. **91**, 4950 (1987).
[21] L. P. Davila, P. Erhart, E. M. Bringa, M. A. Meyers, V. A. Lubarda, M. S. Schneider, R. Becker, and M. Kumar, Appl. Phys. Lett. **86**, 161902 (2005).
[22] T. Hatano, Phys. Rev. Lett. **93**, 085501 (2004).
[23] J. P. Hirth and J. Lothe, *Theory of Dislocations* (Wiley, New York, 1982), Chap. 10.1, pp. 306–320.
[24] K. S. Chueung and S. Yip, J. Appl. Phys. **70**, 5688 (1991).
[25] J. Cormier, J. M. Rickman, and T. J. Delph, J. Appl. Phys. **89**, 99 (2001).
[26] J. A. Zimmerman, E. B. Webb III, J. J. Hoyt, R. E. Jones, P. A. Klein, and D. J. Bammann, Modell. Simul. Mater. Sci. Eng. **12**, S319 (2004).
[27] M. H. Sadd, *Elasticity: theory, applications and numeric* (Elsevier Inc. 2005), Chap. 8.4, p. 163.
[28] G. Simons and H. Wang, *Single Crystal Elastic Constants and Calculated Aggregate Properties* (MIT Press, Cambridge, MA, 1977), p. 21.